Article

Not peer-reviewed version

Exploring the potential of silica fume and micro-quartz for enhancing the strength, durability, and sustainability of cementitious concrete

Mohammad Iqbal Khan * , Yassir M. Abbas , Galal Fares

Posted Date: 9 October 2023

doi: 10.20944/preprints202310.0448.v1

Keywords: Concrete, micro-quartz, permeability, porosity, silica fume, strength.

Article

Exploring the Potential of Silica Fume and Micro-Quartz for Enhancing the Strength, Durability, and Sustainability of Cementitious Concrete

Mohammad Iqbal Khan *, Yassir M. Abbas and Galal Fares

Department of Civil Engineering, King Saud University, P.O. Box 800, Riyadh 11421, Saudi Arabia
* Correspondence: miqbal@ksu.edu.sa

Abstract: This study aims to formulate binary cementitious systems containing silica fume (SF) and micro quartz (MQ) to improve cementitious concrete's durability and mechanical properties. In this investigation, we examined the effects of different essential variables, such as the level of SF and MQ replacement and the ratio of the water-binder (w/b). In this study, the w/b ratios were 0.25, 0.3, 0.35, and 0.4. Replacement levels for SF were 8, 10, and 12%, while replacement levels for MQ were 5, 8, 10, 15, 25, and 35%. The porosity and permeability decreased with an increase in replacement levels, regardless of the type of fine material used or the amount of replacement. Meanwhile, the strength increased markedly with SF replacement, reaching its maximum MQ of 25% at the SF level. The strength of the SF mixing was the highest in all mixes, and it remained the highest until 15% of MQ was replaced. The ultrafine size of MQ particles contributes to the improvement of compressive strength, porosity, and permeability in a similar way to SF particles, despite their high crystalline structure. Furthermore, in this study, analysis of variance (ANOVA) was employed to verify the influence of each variable on the studied response.

Keywords: concrete; micro-quartz; permeability; porosity; silica fume; strength

1. Introduction

1.1. Background

Advances in construction technology emerge from the advantages of the latest concrete technology. Since its first use, concrete has become a mandatory gigaton material for various construction and structural applications. The estimated worldwide concrete production has reached 30 gigatons [1]. The boom in construction witnessed in the current century has increased the demand for concrete materials, especially cement as the essential binding material. Aïtcin [2] reported that the demand for cement increased from 10 Mt in 1900 to 3.5 Mt until 2016, this increases with the demand for concrete for new constructions. The main ingredients of concrete can be seen as those composing the cementitious matrix and those forming the skeletal aggregates [3–5]. The first phase, the cementitious matrix, is responsible for drying shrinkage and most of the deteriorating reaction when innocuous aggregates are present. The critical zone is represented by the boundaries between the cementitious matrix and aggregate circumferences, which lead to the formation of local stresses along the interface due to shrinkage and hardening processes as weak points [3]. The cracks are well reported to be initiated due to and near these weak points. Accordingly, the overall durability depends on the quality of the interfacial transition zone (ITZ) and its microstructure [6–8]. Therefore, improving the quality of ITZ becomes a common practice to enhance the durability of concrete. The improvement process can be achieved by reducing the water-to-binder (w/b) ratio and applying appropriate chemical and mineral admixtures, as well as many other fine and ultra-fine natural and artificial materials.

1.2. Bibliographical overview

Preprints (www.preprints.org) | NOT PEER-REVIEWED | Posted: 9 October 2023 doi:10.20944/preprints202310.0448.v1

According to Lagerblad and Kjellsen [9] and Winnefeld [10], the factors affecting the quality of ITZ are:

- Type of cement and, accordingly, its chemistry and activity.
- The packing of both the ingredients for the cementitious matrix and aggregate skeleton
- Chemical and volume stability of the individual cementitious, mortar, and concrete phases.
- Sieve analysis, fineness, and chemical stability of fine and coarse aggregates.

Packing density comes from the main concept of filling the voids in the cementitious matrix using finer powders and those in the aggregate skeleton using well-distributed aggregates. Dispersion becomes critical for optimal packing density, which can be achieved using compatible chemical admixtures. Mineral admixtures with pozzolanic activities contribute to the formation of secondary calcium-silicate hydrates (C-S-H), which enhance the quality of ITZ. Moreover, the presence of mineral admixtures modifies the flowability of concrete due to the slippage of aggregates, causing it to move from a normal slump to a high degree of flowability. The improved flowability is reported to lead to improved ITZ [11]. The presence of filling particles, either smaller than cement particles or aggregate grains, can be visualized, as shown in Figure 1.

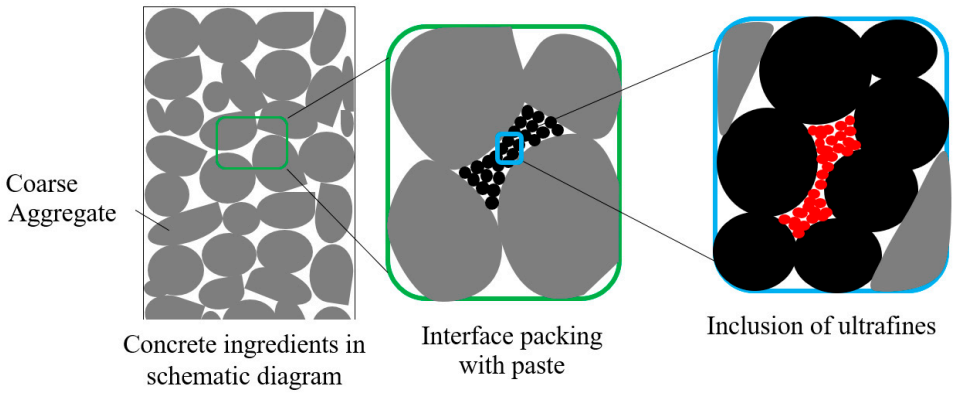

Figure 1. The addition of ultrafine fillers improves the packing of concrete.

The partial replacement of cement with mineral admixtures was shown to have multiple economic and durability benefits. For example, silica fume (SF) has a high degree of pozzolanicity due to its particles with nano-median sizes (200–400 nm) and a high degree of amorphicity. When SF partially replaces cement, it first reduces the amount of cement. It thus reduces the CO_2 footprint, and second, it reacts with the liberated calcium hydroxide (CH) due to the hydration of silicate phases and the formation of C-S-H. This chemical reaction significantly improves the mechanical properties of concrete due to the elevated strength of the cementitious matrix and the enhanced ITZ properties [12–14]. SF replacement level of up to 15% was reported to be used in the production of high-performance concrete (HPC) with improved strength [15–17]. Compared to the control mixture, the presence of up to 15% SF is also reported to lead to an increase of 21% in the compressive strength that reaches its maximum improvement value at 90 days [15]. Similarly, it is also reported that the incorporation of 6 and 10% SF has led to a 19% and 25% increase in compressive strength, respectively [18]. In another study, the early strength was reduced compared to the control mix due to the presence of SF at low w/b ratios of 0.27 to 0.33 and the improvement was noted after 7 days [19]. The reduction was notable at a higher replacement level. This can be attributed to the difficulty of efficiently dispersing SF at higher dosages, which can also be attributed to the increase in plastic viscosity and yield stress that make the flowability difficult and the packing density lower. All the researchers agreed that the increase in strength could be attributed to the pozzolanicity and filling effect of the nano-sized SF particles.

On the other hand, fly ash (FA) is another type of mineral admixture known for its amorphous alumino-ferrite-silicate structure and especially spherical structures known as cenospheres. Due to the micro size of its particles, they become slower in the pozzolanic activity with CH compared to SF. Due to the slow pozzolanic activity of FA, its incorporation in a partial replacement of cement causes

 doi:10.20944/preprints202310.0448.v1

a notable reduction in the heat of hydration of cement. Therefore, due to its pozzolanic activity and spherical structure, the presence of FA has the dual benefits of secondary hydration and filler [20–25].

For that reason, the effective combination of FA and SF as a partial replacement for cement and an enhancer for strength and durability becomes a common practice [26–34]. The ternary combination of SF (10%) with FA increases its compressive strength compared to the reference binary with FA by about 145% [29]. The ranges of 8–12% SF and 15–20% FA were reported to significantly reduce the permeability and related properties such as porosity and sorptivity [26]. Similarly, it is mentioned that the ranges of 4–8% SF and 20–50% FA could be combined together in different ternary mixes for better mechanical properties and the lowest permeability [35]. For example, the combination of 3% SF and 32% FA was found to have a chloride permeability of 3000 coulombs, while it was found to have one below 500 coulombs when formulating 9% SF and 26% FA [36,37]. Therefore, the proportion of binding materials and curing conditions have a substantial effect on the ITZ and durability properties of fillers and materials of variable pozzolanic properties [38–40]. The filler effect due to the size effect can also be attributed to the formation of different nucleation sites that accelerate cement hydration products with condensed and improved microstructures [10,41–44]. Therefore, the packing density at the cementitious matrix and aggregate skeletal levels, in addition to the nature of fine and ultrafine powder, all together represent an overall package that defines the final output's fresh and hardened properties [45–47]. Despite all these old and recent investigations, ultrafine powders, especially silica sand, still need further research.

1.3. Scope and significance of the research

From the previous literature review, it becomes evident that there is limited literature on the use of ultrafine fillers for improving concrete's durability. This study aimed to examine the mechanical and durability properties of concrete using different ultrafine fillers and mineral admixtures both alone and in binary combinations. In this study, we focused on the effects of micro-quartz filler (MQ), in combination with silica fume, on the properties of various concrete types, including high-, and normal-strength concrete mixes. This study examined 40 concrete mixes containing varying ratios of water–binder (0.25, 0.30, 0.35, and 0.40) and binary combinations of both SF and MQ to optimize their strength and durability characteristics. In this comprehensive study, the integration of silica fume and micro-quartz not only innovatively enhances concrete's durability and mechanical characteristics but also positions it as a leading sustainable construction solution.

2. Materials

This study used ordinary Portland cement (PC-type I, which meets ASTM C 150) as the primary binder. Supplementary cementitious material, namely silica fume (SF), has also been included. Additionally, micro-quartz (MQ) as ultrafine filler was added to the concrete mixes to improve their strength and durability. In this investigation, PC, SF, MQ, and median grain sizes were approximately 13.0, 8.0, 3.5, and 15.0 μm. Table 1 lists the physicochemical properties of the fine powders, and Figure 2a shows their grain size distributions.

Table 1. The physicochemical properties of the fine powders.

Oxide composition (%)	PC	SF	MQ
SiO_2	20.2	93.2	99.5
Al_2O_3	5.49	0.2	0.20
Fe_2O_3	4.12	0.03	0.03
CaO	65.43	0.72	0.01
MgO	0.71	0.14	-
Na_2Oeq	0.26	0.07	-

Preprints (www.preprints.org) | NOT PEER-REVIEWED | Posted: 9 October 2023 doi:10.20944/preprints202310.0448.v1

SO_3	2.61	<0.01	-
Loss on ignition (%)	1.38	5.4	-
Specific gravity	3.14	2.27	-
Fineness (m^2/kg)	373	19,000	16,500

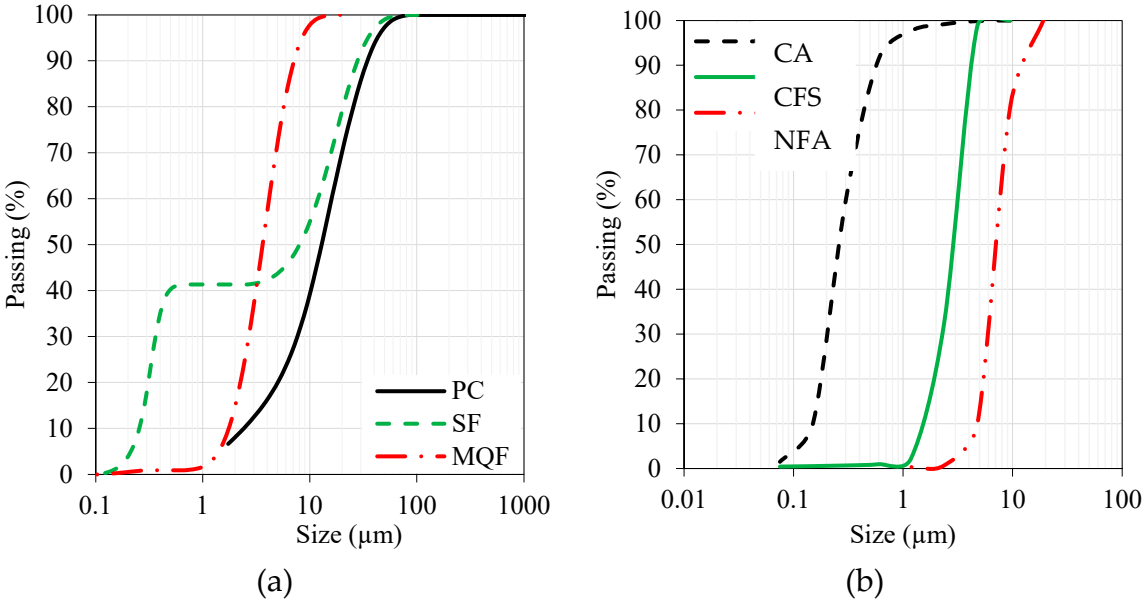

Figure 2. The grain size distribution of (a) fine powders, and (b) aggregates.

Images of the fine powders obtained by scanning electron microscopy (SEM) are presented in Figure 3. The MQ particles in Figure 3a are characterized by their amorphous shape, and their average size ranges from 2 to 5 μm. Additionally, Figure 3b illustrates the SEM analysis of the SF which contained a mixture of smooth and rough-surfaced sphere particles with a mean size of 10 μm, significantly smaller than the typical SF particle size that is typically less than 1 μm, according to [48]. Moreover, the PC particles were polyangular, asymmetrical, and ranged in size from 1 to 20 μm [Figure 3b]. Additionally, Figure 3c illustrates that the FA particles exhibit sphere-shaped shapes with a mean particle size of approximately 15 μm.

Preprints (www.preprints.org) | NOT PEER-REVIEWED | Posted: 9 October 2023 doi:10.20944/preprints202310.0448.v1

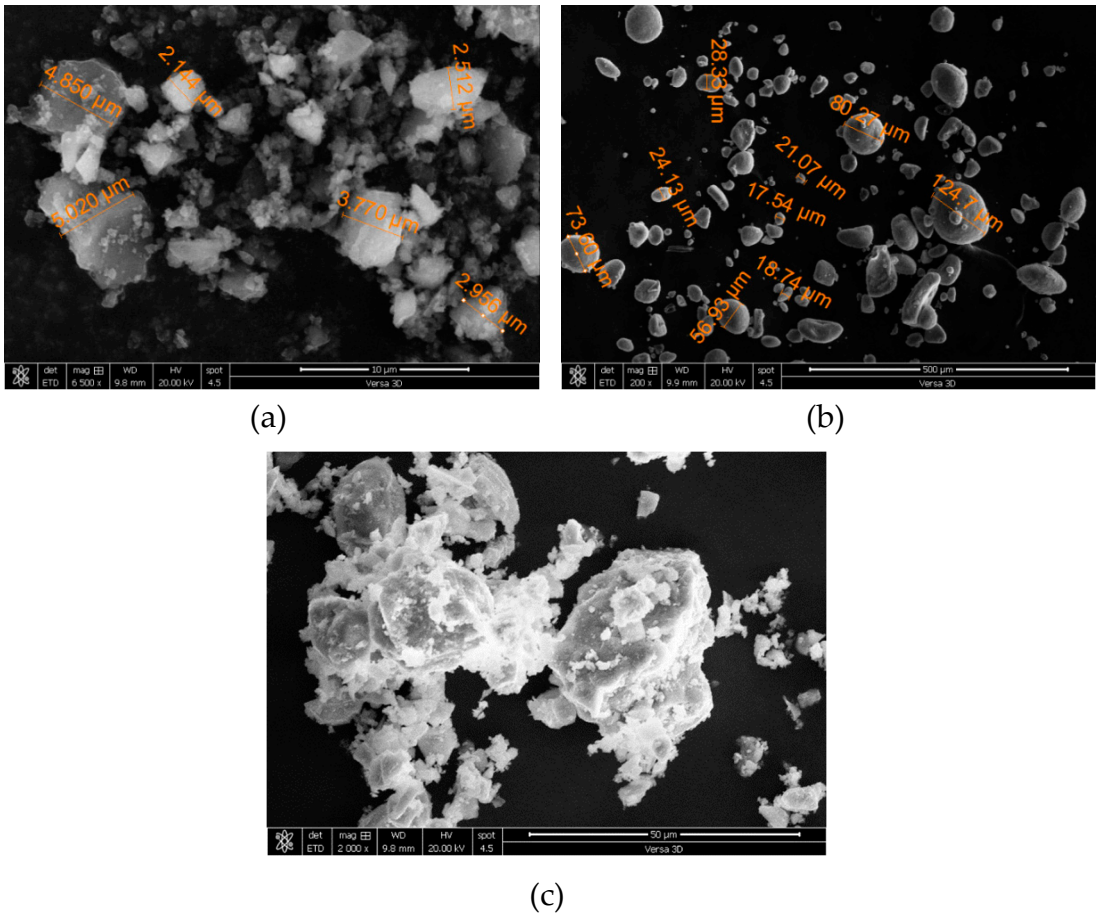

Figure 3. SEM images of: (a) MQ, (b) SF, and (c) PC.

This study utilized a modified polycarboxylic ether polymer superplasticizer (SP) known as Glenium 51 to achieve the required workability of concrete mixes. The dry extract of this SP is 36% and its specific gravity is 1.1. To calculate the SP dosage for the concrete mixture, a ratio of the dry extract (D.E.) and the cement weight (%, wt.) was divided, and this ratio was optimized for a concrete mixture that would provide the highest workability. In this investigation, we used two types of sand with varying particle sizes to prepare the concrete mixes, namely crushed fine aggregates (CFA) and natural fine aggregates (NFA). These fine aggregates were characterized by fineness moduli of 4.66 and 1.47, respectively. In the blended fine aggregates, the fineness modulus was 2.54 as a result of the combination of 65% NFA and 35% CFA. Furthermore, coarse aggregates (CA) with an aggregate size of not more than 10 mm have also been used in the preparation of all concrete mixtures. Figure 2b illustrates the grain size distribution of the aggregates, while Table 2 summarizes their physical properties.

Table 2. The physical properties of the aggregates.

Material	Specific Gravity	Absorption, %	Unit Weight, kg/m³
NFA	2.63	0.77	1725
CFA	2.68	1.52	1552
CA	2.65	1.45	1570

3. Methodology

3.1. Mixing, casting, and curing

Preprints (www.preprints.org) | NOT PEER-REVIEWED | Posted: 9 October 2023 doi:10.20944/preprints202310.0448.v1

In this study, the various aggregates were stirred in a typical concrete mixer for a few minutes while the associated absorption water was introduced simultaneously. Afterward, the fine powders were mixed dry for a few minutes to ensure uniformity. Then, the mixing water and SP solution were combined as a ready-mixed blend and stirred for three minutes, followed by a three-minute break and a second two-minute stir. On the other hand, a fiber-reinforced concrete system was developed by incorporating fibers during concrete preparation and blending it for five minutes to distribute the fibers evenly. A separate procedure was carried out in the HPFRCC, in which the dry materials were mixed together in an effort to form a unified material and a pre-mixed amount of SP dosage was added to the mixture until a unified material was formed. As in this case, the mixing process continued until a homogenized mixture had been achieved. Upon attaining this condition, fibers were added, and it was mixed until the fibers were dispersed and thoroughly incorporated into the composite. Finally, the mixer was turned off, and the specimens were cast into the molds, which concluded the mixing process. In Table 3, detailed characteristics of specimens cast from different cement-based materials are presented to assess their properties. To maintain the specimen's moisture condition, a trowel was used to smooth the top surface and a plastic sheet was placed to cover it. In this investigation, the following curing methods have been employed. In all these curing systems, specimens were demolded after 24h and the curing regime was implemented up to the testing age. Notably, the Hot room curing system was employed for the drying shrinkage testing.

- Standard curing: the specimens were cured in a humidified environment (at 22°C and 100% RH).
- Hot room curing: the samples were cured in the hot room (at 40±2°C and a 10–20% RH).

Table 3. Detail of the cylindrical specimens for material testing.

Test	**Uniaxial compression**	**Rapid chloride-ion permeability**
specimen dimensions (mm)	$D = 100$ $L = 200$	$D = 50$ $L = 100$

3.2. Detail of mixes

This study examined 40 concrete mixes containing SF and MQ to determine the optimal mixture for strength and durability. Table 5 displays a detailed breakdown of these different mixes' water-binder ratios and fine powder contents. The CA content of these mixes was 1056 kg/m^3, while the total FA content of these mixes was 450±40 kg/m^3. The SP for these mixes ranged from 4.3 to 12.6 L/m^3, which was adjusted to maintain the slump (measured in accordance with ASTM C 143) within a reasonable range (175±25 mm). A notable feature of the concrete casting process is the measurement of the unit weight of the concrete to determine its density. Figure 4 illustrates the measurements of these mixes with unit weights ranging from 2361.4 to 2481.4 kg/m^3, with a mean value of 2418.4 kg/m^3.

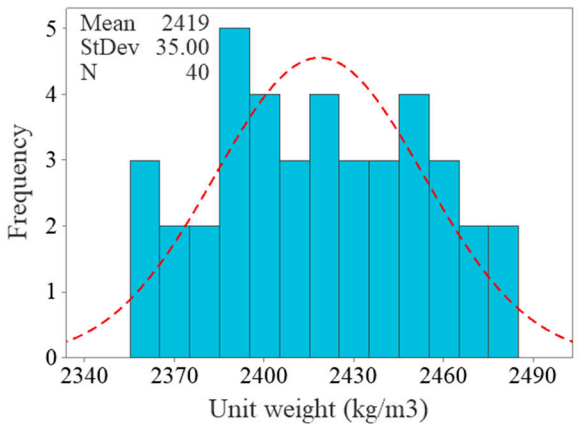

Preprints (www.preprints.org) | NOT PEER-REVIEWED | Posted: 9 October 2023 doi:10.20944/preprints202310.0448.v1

Figure 4. Unit weight of the developed concrete mixes.

Table 4. Details of concrete mixes.

Sr. No.	Mix ID	w/b	Fine powders				Sr. No.	Mix ID	w/b	Fine powders			
			PC	SF	MQ	Total				PC	SF	MQ	Total
			(kg/m³)							(kg/m³)			
1	CTRL-25	0.25	550			550	21	CTRL-35	0.35	450.0			450
2	SF08-25		506	44.0		550	22	SF08-35		414.0	36.0		450
3	SF10-25		405	45.0		550	23	SF10-35		495.0	55.0		550
4	SF12-25		484	66.0		550	24	SF12-35		352.0	48.0		400
5	MQ05-25		523		27.5	550	25	MQ05-35		427.5		22.5	450
6	MQ08-25		506		44.0	550	26	MQ08-35		414.0		36.0	450
7	MQ10-25		405		45.0	450	27	MQ10-35		495.0		55.0	550
8	MQ15-25		468		82.5	550	28	MQ15-35		382.5		67.5	450
9	MQ25-25		413		137.5	550	29	MQ25-35		337.5		112.5	450
10	MQ35-25		358		192.5	550	30	MQ35-35		292.5		157.5	450
11	CTRL-30	0.30	500			500	31	CTRL-40	0.40	400.0			400
12	SF08-30		460	40.0		500	32	SF08-40		368.0	32.0		400
13	SF10-30		360	40.0		400	33	SF10-40		450.0	50.0		500
14	SF12-30		440	60.0		500	34	SF12-40		396.0	54.0		450
15	MQ05-30		475		25.0	500	35	MQ05-40		380.0		20.0	400
16	MQ08-30		460		40.0	500	36	MQ08-40		368.0		32.0	400
17	MQ10-30		360		40.0	400	37	MQ10-40		450.0		50.0	500
18	MQ15-30		425		75.0	500	38	MQ15-40		340.0		60.0	400
19	MQ25-30		375		125.0	500	39	MQ25-40		300.0		100.0	400
20	MQ35-30		325		175.0	500	40	MQ35-40		260.0		140.0	400

3.3. Testing procedures

3.3.1. Uniaxial compression test

Preprints (www.preprints.org) | NOT PEER-REVIEWED | Posted: 9 October 2023 doi:10.20944/preprints202310.0448.v1

A thin layer of sulfur mortar was applied to the cylindrical specimens before performing the uniaxial compression test. This ensures that the top and bottom surfaces are flat, thus ensuring the load will be equally distributed. In this study, the 28d elasticity modulus and the compressive strength of cement-based materials were assessed according to the specifications of ASTM C469 and ASTM C39, respectively. The test was conducted on a ToniTech universal compression testing machine (capacity 3000 kN, See Figure 4). Two linear variable displacement transducers (LVDTs) and compressometer rings were attached at approximately 100 mm (the center height of the samples) to quantify in-plane and transverse strains. The loading conditions in this study were displacement- and load-controlled (i.e., 2.5×10^{-3} mm/s and 0.25×MPa/s respectively). We conducted the measurements for two or three duplicates of the compression test samples in order to ensure reliability, while the mean result is reported.

(a) (b)

Figure 4. The uniaxial compression test: (a) schematic diagram and (b) testing setup.

3.3.2. Rapid chloride-ion permeability test

Following ASTM C1202, we performed a chloride permeability test on concrete cylinders with diameters of 50 mm and lengths of 100 mm. As recommended by RELIM [49], these cylindrical concrete samples were vacuum-soaked to maintain continuous saturation levels. In terms of analyzing diffusion characteristics, the chloride permeability test does not provide an accurate measure of these characteristics [32]. Nevertheless, this test can be used to examine parametric data in the context of this study. Figure 1 illustrates how concrete cylinders are filled with chloride before the test is conducted in order to measure the concrete's chloride permeability. We conducted the measurements on two or three duplicates of the chloride permeability sample in order to ensure the reliability and repeatability of the results of this study.

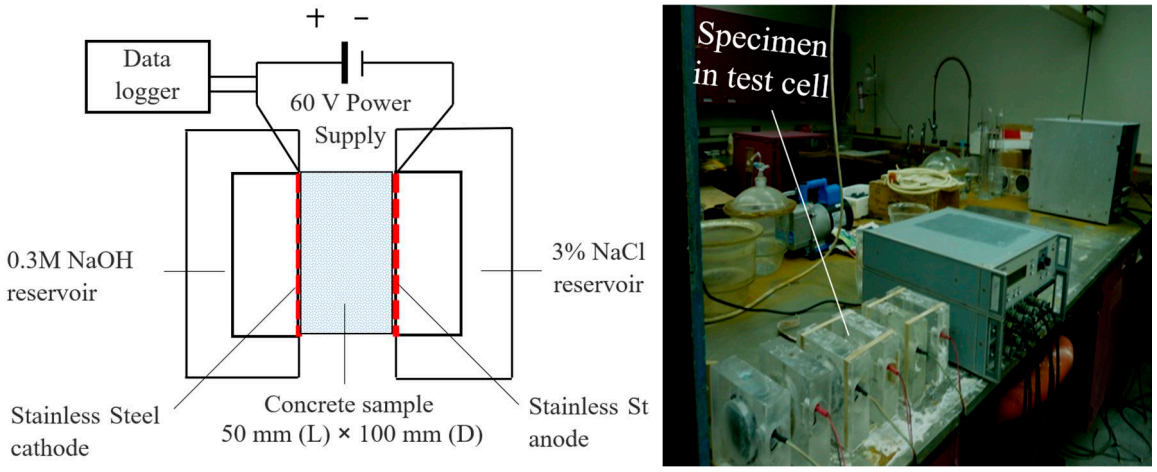

(a) (b)

Preprints (www.preprints.org) | NOT PEER-REVIEWED | Posted: 9 October 2023 doi:10.20944/preprints202310.0448.v1

Figure 5. Rapid chloride-ion permeability test: (a) schematic diagram and (b) testing setup.

3.3.3. Porosity test

In this study, concrete's porosity was evaluated in accordance with RILEM CPC 11.3. To accomplish this test, a disc concrete specimen (100 mm diameter with 50 mm height) was dried at 100 ±5°C until a constant weight was obtained. We placed dried concrete samples under a vacuum in a desiccator for three hours, then immersed them in de-aired distilled water for another hour, followed by an additional immersion in the desiccator. Accordingly, we were able to calculate the porosity of concrete as a result of Eq. (1).

$$\text{Porosity}(\%) = \left[\frac{M_3 - M_1}{M_3 - M_2}\right] \times 100 \quad (1)$$

Where, M_3 is the mass of water-saturated concrete specimen in air, M_1 is a mass of the oven-dried concrete specimen, M_2 is the mass of the concrete specimen in water.

4. Results and discussion

The results of the experiments conducted in this study are summarized in Table 6. In the following sections, we will discuss the results of the experiment in more detail.

Table 5. Summary of the experimental results.

Mix ID	Strength (MPa)				Porosity	Permeability Coulombs
	7d	28d	180d	400d	%	
CTRL-25	70.4	89.9	93.0	96.0	7.9	1433.3
MQ05-25	71.6	91.7	95.5	101.0	7.0	1169.0
MQ08-25	74.1	93.4	97.4	105.3	6.3	893.7
MQ10-25	68.8	85.8	90.9	95.8	5.4	699.3
MQ15-25	64.7	80.8	88.7	96.1	4.7	460.0
MQ25-25	51.6	77.3	86.7	93.9	3.0	97.7
MQ35-25	49.0	70.9	85.6	92.2	2.7	61.7
SF08-25	66.7	91.8	94.4	97.1	4.2	332.7
SF10-25	69.0	94.9	95.9	97.9	3.6	235.3
SF12-25	72.1	98.1	98.2	99.3	3.1	150.0
CTRL-30	60.4	77.7	83.9	88.6	8.1	2400.7
MQ05-30	62.0	80.0	84.1	92.1	7.6	1502.3
MQ08-30	63.4	81.4	87.1	96.9	7.0	885.7
MQ10-30	57.4	75.4	82.4	89.9	6.2	753.3

 doi:10.20944/preprints202310.0448.v1

MQ15-30	53.1	68.8	78.6	88.7	5.9	553.3
MQ25-30	44.1	67.5	75.5	84.7	5.2	167.0
MQ35-30	41.9	61.5	72.3	81.4	4.3	89.7
SF08-30	57.8	79.5	80.9	83.9	5.5	413.7
SF10-30	59.4	81.7	85.2	86.9	5.3	332.7
SF12-30	62.8	86.4	87.1	88.0	4.0	312.7
CTRL-35	52.7	69.5	74.9	79.4	9.2	2814.7
MQ05-35	53.8	71.8	80.8	84.4	8.8	1936.7
MQ08-35	55.5	74.3	85.0	90.2	8.6	1406.0
MQ10-35	50.5	63.8	75.3	78.5	8.0	1125.0
MQ15-35	49.3	57.8	68.0	74.1	7.5	997.5
MQ25-35	40.0	54.6	63.1	72.1	6.6	544.7
MQ35-35	34.3	49.8	56.4	65.9	6.5	296.7
SF08-35	54.1	73.6	75.0	80.1	6.7	523.0
SF10-35	53.2	74.2	77.4	83.3	6.3	483.0
SF12-35	56.7	77.8	78.4	75.5	6.1	423.7
CTRL-40	46.7	59.2	61.8	65.4	11.3	3437.0
MQ05-40	48.0	61.0	66.2	71.1	10.2	2453.0
MQ08-40	49.9	63.2	69.2	76.1	9.6	1886.7
MQ10-40	43.6	53.7	60.4	65.7	8.9	1404.0
MQ15-40	39.7	49.6	58.7	64.2	8.5	1080.3
MQ25-40	31.6	44.8	53.8	60.8	8.0	847.0
MQ35-40	28.9	42.8	50.5	60.0	7.2	323.0
SF08-40	47.8	64.2	67.8	72.9	7.4	851.3
SF10-40	48.0	65.6	69.5	74.5	7.1	782.7
SF12-40	51.0	69.9	70.9	71.8	6.9	740.0

4.1. Strength characteristics

Preprints (www.preprints.org) | NOT PEER-REVIEWED | Posted: 9 October 2023 doi:10.20944/preprints202310.0448.v1

4.1.1. The 28d compressive strength of SF and MQ concrete

Figures 7 and 8 illustrate the influence of MQ and SF on the 28d compressive strength of concrete mixes developed with a variety of water-binder ratios (0.25, 0.30, 0.35, and 0.40). Figure 7 shows that compression strength was almost unaffected with ultrafine replacement rated at less than 10% in the concrete matrix regardless of the water-cement ratio. We also noticed that compressive strength increased slightly when 8% of cement was replaced with ultra-fine material. The 28d's compressive strength decreases, however, if the ultrafine dosage reaches 10% or more. In the presence of increasing water-binder ratios, this decrease in compressive strength becomes more apparent. In the case of the 0.4 water-cement ratio, the 28d strength was reduced by 10, 16, 24, and 28% for MQ replacement levels of 10, 15, 25, and 35%, respectively. A lower level of pozzolanitivity in the MQ may explain this reduction in compressive strength. The presence of micro-packing effects could explain the lack of reductions or even slight increases at low MQ doses. A noteworthy aspect of this conclusion is that it corresponds to the conclusions of other researchers [50–54].

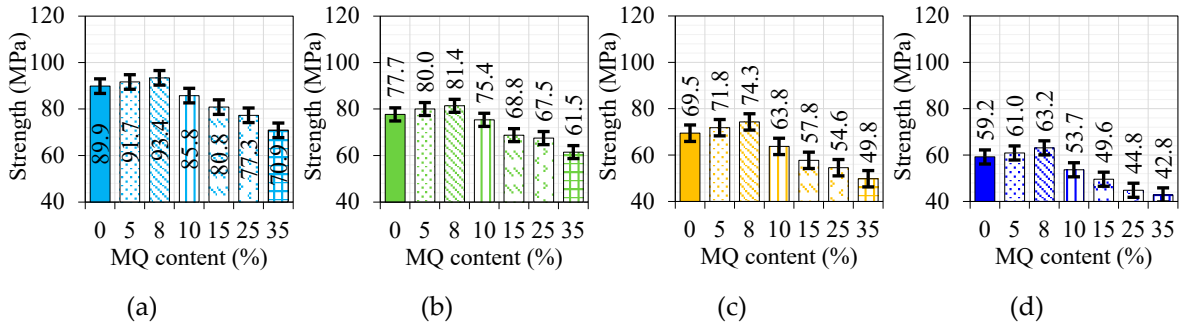

Figure 7. The impact of the MQ content on the 28d compressive strength with (a) 0.25, (b) 0.30, (c) 0.35, and (d) 0.40 water–binder ratio.

Typically, silica fume is used to enhance the properties of cement-based materials; therefore, it is used predominantly in high-performance concrete due to its fineness and pozzolanic reaction. Figure 8 illustrates the 28d compressive strength of concrete has been increased by the addition of 8, 10, and 12% SF for four different ratios of water–binders (0.25, 0.3, 0.35, and 0.4). The compressive strength increased by 2, 5, and 9% with SF replacements of 8, 10, and 12% at a water-binder ratio of 0.25. Further, when cement was replaced by SF at a dosage of 8, 10, and 12% at a water-cement ratio of 0.3, the increase in compressive strength was 3, 5, and 11%. The compressive strength was increased by 6, 7, and 12% when SF was substituted for cement at dosages of 8, 10, and 12% using a water-binder ratio of 0.35. Further, the compressive strength was significantly boosted by 8.5, 11, and 18% when SF was substituted for cement at dosages of 8, 10, and 12% using a water-binder ratio of 0.4. There have been several studies stating that concrete strength can increase by 30 to 100% depending on many factors such as mix type, cement type, SF dosage, superplasticizer, aggregates, and curing regime [55–58]. In concrete, SF particles improve packing by filling in the spaces between the particles. In the same way, and fills gaps between coarse aggregates when it is mixed with cement. These findings showed that the maximum 28d strength of concrete (18%) was obtained with 12% SF and 0.4 water-binder ratio. As the water-binder ratio increases, the incorporation of SF appears to be more effective at enhancing concrete strength. The higher the water-binder ratio, the more porous the concrete becomes, which makes SF an extremely valuable component of increasing strength due to its micro-filling effect. It is true that concrete that has a low water-binder ratio, like that of 0.25 or 0.30, is pretty compact, but the fine particles still contribute to the strength of the mix. The major role the SF would play in a scenario like this would be to enhance the flowability of the concrete during its plastic phase. It has been scientifically proven that filling the spaces between cement grains occurs whenever there is sufficient SP available to counteract the electrostatic forces between the particles of cement [59,60].

Preprints (www.preprints.org) | NOT PEER-REVIEWED | Posted: 9 October 2023 doi:10.20944/preprints202310.0448.v1

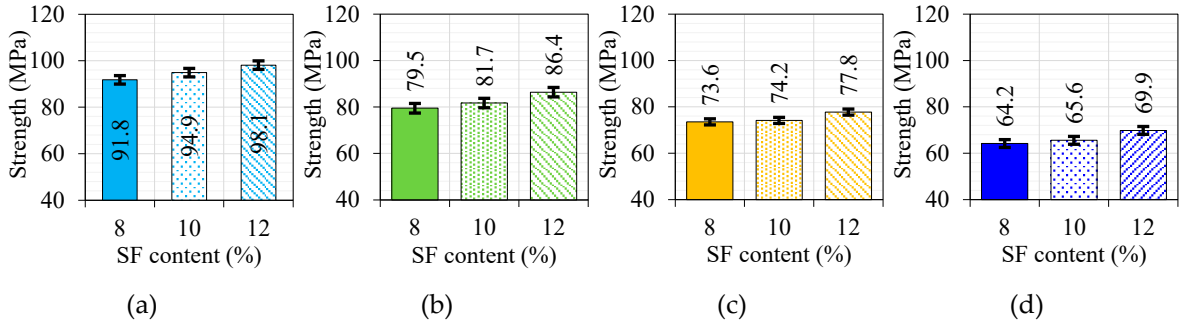

Figure 8. The impact of the SF content on the 28d compressive strength with: (a) 0.25, (b) 0.30, (c) 0.35, and (d) 0.40 water–binder ratio.

4.1.2. A modified ABRAM's model for SF and MQ concrete

In the second decade of the 20th century, Abram [61] developed a relationship between the compressive strength and water–cement ratio of normal Portland cement concrete are related (Eq (1), where $A = 96.6$ and $B = 8.2$ [62,63]. The development of this relationship was considered a significant step in concrete technology [62]. There are a number of factors that contribute to the strength of concrete. The factors are classified by Newman [57] into three categories: (i) properties and ingredients of constituent materials, (ii) curing system, and (iii) testing parameters. In order to understand how concrete responds to stress, various factors must be understood. It is therefore essential to formulate an exact formula for the prediction of the compressive strength of any modified concrete in order to determine its strength. In the present study, a modification factor (α) is introduced into Abram's formula [Eq (2)]. This modification factor was calculated using the most closely fitting experimental data for all mixtures.

$$f_c' = \frac{A}{B^x} \tag{1}$$

$$f_c' = \alpha \frac{A}{B^x} \tag{2}$$

Where,

f_c' : the concrete's compressive strength at a certain age (here, considered 28d).

A and B : the empirical-based factors reflect the effects of individual constituent materials, the curing system, testing parameters, and the age of concrete.

x : the water–binder ratio.

Figure 9 shows the prediction capacity of the proposed formula [Eq. (2)] for the water–binder and 28-day compressive strength of MQ and SF concrete's strength relations. The alpha value for the MQ concrete was determined to be 1.32, whereas the alpha value for the SF concrete was determined to be 1.60. Figure 9a illustrates that most MQ concrete points fall within the error range of ±15%, in contrast to Abram's formula [Eq. (1)] which underestimated concrete strength. In addition, Figure 9b reveals that SF concrete data points fall within the ±5% error band of the proposed model, while Abram's distinctly underestimates it.

Preprints (www.preprints.org) | NOT PEER-REVIEWED | Posted: 9 October 2023 doi:10.20944/preprints202310.0448.v1

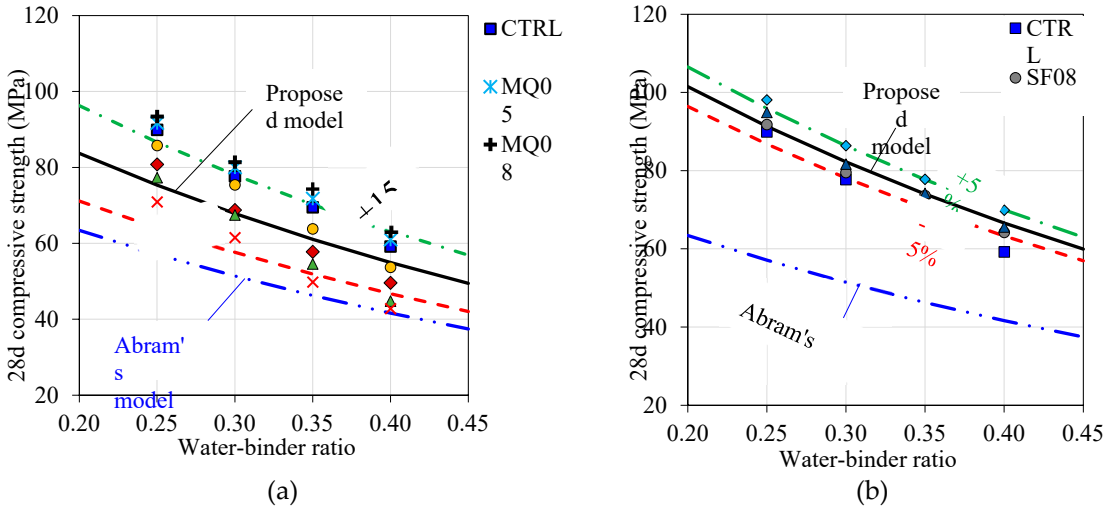

Figure 9. 28d compressive strength vs. water–binder ratio: (a) MQ, and (b) SF concrete.

4.1.3. The age-dependent compressive strength

A number of factors determine the age-dependent strength of concrete, namely the type of cement used, the type of admixtures used, the water-binder ratio, and weather conditions [64]. The relationship for strength as a function of time assumes moist curing and normal temperature (20°C). Assuming a constant water–binder ratio, it was predicted that higher strength would be achieved by exposing the cement to moist curing conditions for a prolonged period of time since anhydrous cement particles undergo hydration during drying. The strength of the material does not significantly increase with time after moisture is removed by capillaries under air-curing conditions [65]. After 28 days, silica fume does not significantly increase compression strength (ACI 234-06). The apparent decrease in compressive strength due to the addition of silica fume to concrete over a period of 90 days has been reported in very limited literature [66].

Based on ACI 234, the impact of testing machines on compressive strength may be the cause of the reduction in strength. In this study, the strength experimental observations at various ages are compared with calculated strengths based on the formulas for time-dependent strength provided by ACI Committee 209 [Eq. (3)] and CEB-*fib*-90 mode code [Eq. (4)]. In Figure 10, the compressive strength of MQ concrete is illustrated as a function of age. In the course of the curing process, MQ ultrafine is found to have a positive effect on the strength gain of concrete, even at higher MQ doses. As a result of the hydration of anhydrous cement particles and the very slow hydration of ultrafine quartz particles, a rise in compressive strength can be explained. According to Figure 10, the inclusion of almost 10% MQ ultrafines in concrete did not adversely affect its strength properties. A possible explanation is that ultrafine grain particles have been packed between cement particles in order to achieve maximum compression strength at the micron level. Further, the ultrafine particles provided the greatest increase in compression strength when added to the system later (after 90 days), regardless of the dosage content. At an early stage (up to 28 days) of concrete development, when a water-binder ratio of 0.35 or 0.40 is used [Figure 10c,d], the concrete's compressive strength decreases with an increased dosage of MQ ultrafine.

$$f_c(t) = \left(\frac{t}{4 + 0.85\,t}\right) f_c' \tag{3}$$

$$f_c(t) = \exp\left[s\left(1 - \sqrt{\frac{28}{t/t_1}}\right)\right] f_c' \tag{4}$$

Where,

Preprints (www.preprints.org) | NOT PEER-REVIEWED | Posted: 9 October 2023 doi:10.20944/preprints202310.0448.v1

$f_c(t)$: mean compressive strength at age t days

s : A coefficient that depends on the cement type (0.20 for high-early strength, 0.25 for normal hardening, and 0.38 for slow hardening).

t_1 : 1-day.

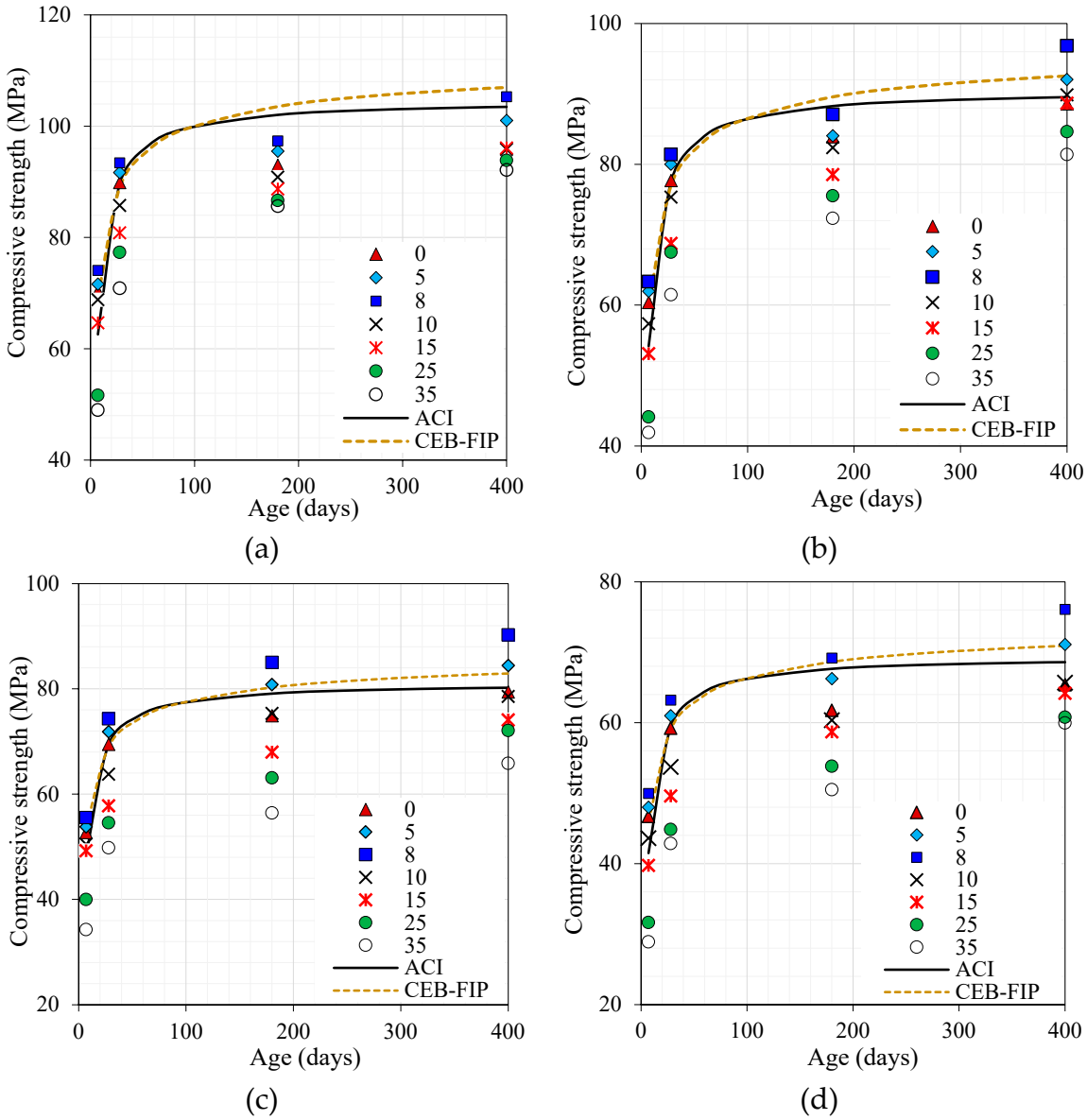

Figure 10. The age-dependent MQ concrete' compressive strength development with: (a) 0.25, (b) 0.30, (c) 0.35, and (d) 0.40 water–binder ratio.

The increase in compressive strength beyond 28 days with the control mix with a water-binder ratio of 0.25 appears to be significantly smaller than that predicted by the ACI Committee 209 and CEB-*fib*-90 model codes, as illustrated in Figure 9a. Nevertheless, the ACI-209 and CEB-*fib*-90 models calculated more accurately the compressive strength gains for MQ concrete with a 0.30 water-binder ratio [Figure 9b].

Figure 11 shows a plot of the development of the compressive strength of SF concrete with a variety of water-binder ratios. As shown in the figure, the replacement of cement with SF has resulted in a significant increase in the early-age strength of concrete compared to control concrete. In the early stages of SF replacement, strength increases may be attributed to (i) a tighter packing of the particles at the micro-scale, and (ii) a chemical reaction between SF and the cementitious matrix.

Preprints (www.preprints.org) | NOT PEER-REVIEWED | Posted: 9 October 2023 doi:10.20944/preprints202310.0448.v1

Further, the ACI-209 and CEB-*fib*-90 predicted the strength of control mixtures nearly perfectly at ages up to 28 days. Nevertheless, at an early age, the compressive strength of SF concrete was higher than that predicted by ACI-209 and CEB-fib-90. Additionally, the compressive strength did not show a significant improvement with aging and was lower than that of the ACI-209 and CEB-FIP models. Several studies [67–69] indicate that many major cement hydration processes occurred during the early stages of cement formation (up to 24 h), which may explain the phenomenon.

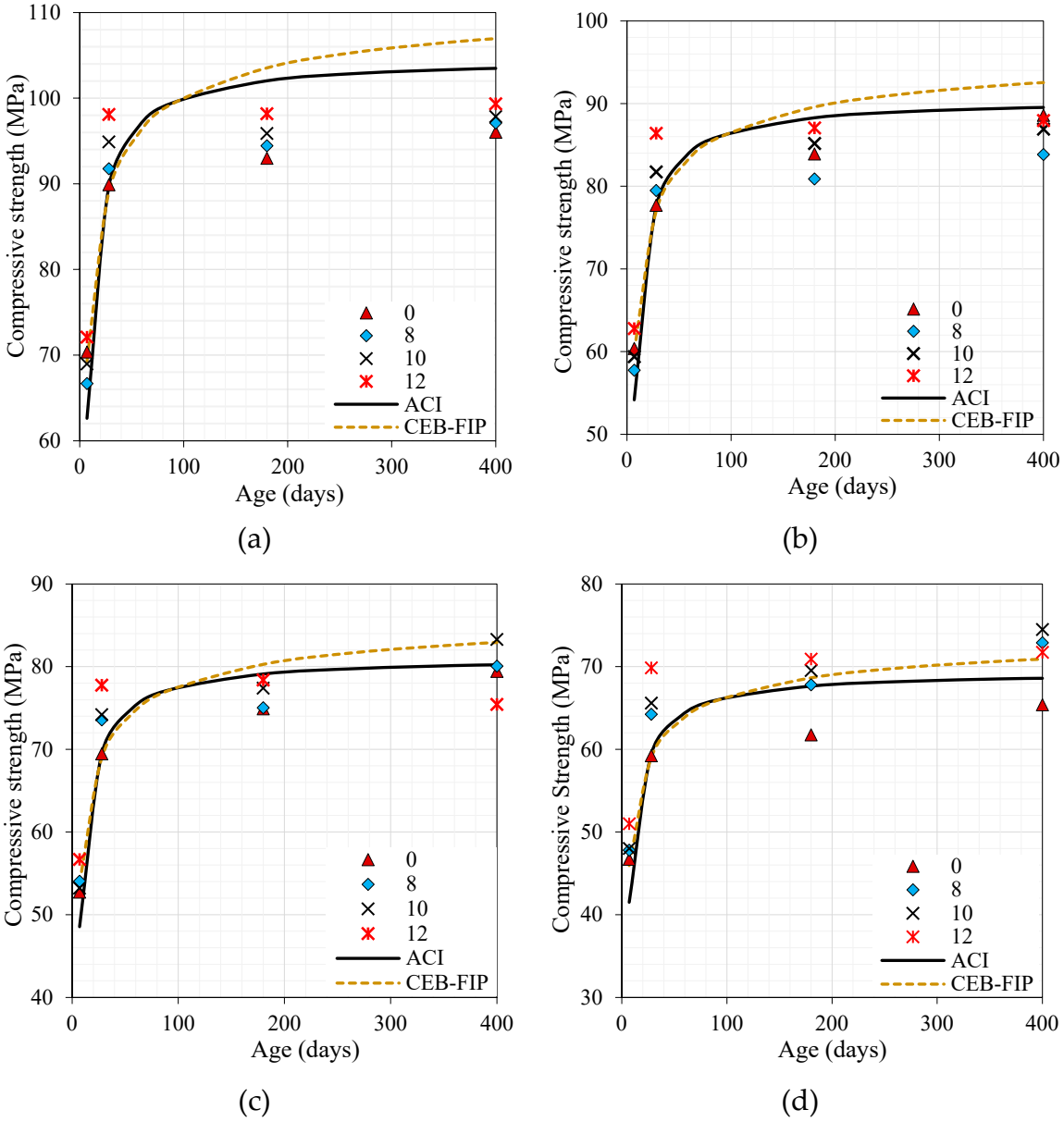

Figure 11. The age-dependent SF concrete' compressive strength development with: (a) 0.25, (b) 0.30, (c) 0.35, and (d) 0.40 water–binder ratio.

In Figure 11, the replacement of cement with MQ and SF ultrafines led to increased compressive strength, indicating a better paste micro-structure, which was apparent from the failure pattern. A typical mode of failure was aggregate fractures, regardless of the water-binder ratio. The paste-aggregate with a lower water-cement ratio was more resistant to loading due to stronger bonding and more compacted interfacial transition zones.

Preprints (www.preprints.org) | NOT PEER-REVIEWED | Posted: 9 October 2023 doi:10.20944/preprints202310.0448.v1

Figure 12. Failure patterns during uniaxial compression loading for: (a) MQ-, (b) SF- concrete.

4.2. Durability characteristics

4.2.1. The chloride-ion permeability

Figure 13 shows the impact of MQ and SF ultrafines on chloride-ion penetration of concrete using different water–binder ratios (0.25–0.40). The ASTM 1202 limits of ion transmission are also shown in the figure to illustrate the range of materials through which chloride ions can be transmitted. The figure shows that the passage of charge through the matrix has been significantly reduced by increasing the ultrafine dosage. The result can be explained by the filling of pores between cement particles with ultrafine materials, which facilitate enhanced packing of the matrix, resulting in a significant reduction in permeability. Further, using 8% MQ ultrafines as a matrix, the passing charge through concrete has been reduced to below the "low limit" for all water-binder ratios. The charge passing through concrete material was lower than the "very low" limit at the water-binder ratio of 0.3 and with 8% MQ ultrafines. Additionally, 15% MQ ultrafines added to concrete resulted in "very low" concrete permeability, regardless of the water-binder ratio. The permeability of concrete and the dosage of MQ generally follow a logarithmic function, as shown in Figure 13a.

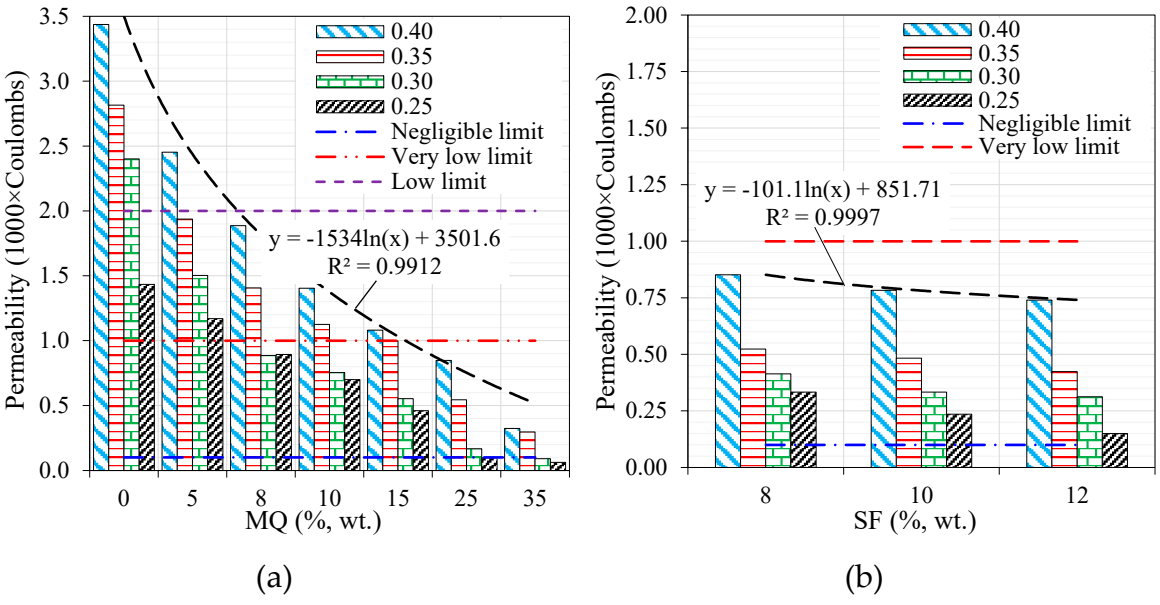

Figure 13. Chloride permeability of: (a) MQ-, and (b) SF-concrete.

Moreover, a significant reduction in the passing charge through the matrix occurred after the addition of SF was observed in Figure 13b. In all water-binder ratios, adding 8% SF resulted in passing

Preprints (www.preprints.org) | NOT PEER-REVIEWED | Posted: 9 October 2023 doi:10.20944/preprints202310.0448.v1

charges through concrete below ASTM 1202's "very low" limit. In addition to being capable of micro-filling concrete, SF also enhances the microstructure of concrete and makes it dense as a result of its pozzolanic reaction. The results of other studies investigated the pozzolanic effects of SF confirmed this improvement in the microstructure [70–73]. Moreover, the permeability of concrete did not improve significantly with an increase in SF dosage from 8 to 12%.

4.2.2. The porosity

Figure 14a illustrates the influence of MQ incorporation into concrete on its porosity at various water–binder ratios. The porosity of concrete mixes with a higher water–binder ratio has been observed to be higher. By increasing the dosage of MQ, a significant reduction in matrix porosity has been observed [Figure 14a]. At higher water-binder ratios, adding MQ to concrete mixtures resulted in less porosity improvement, perhaps due to reduced cement content in concrete mixtures and therefore fewer micropores. At lower ratios, however, the improvement in porosity is more pronounced. In general, the porosity of concrete and the MQ dosage were exponentially related [Figure 14a].

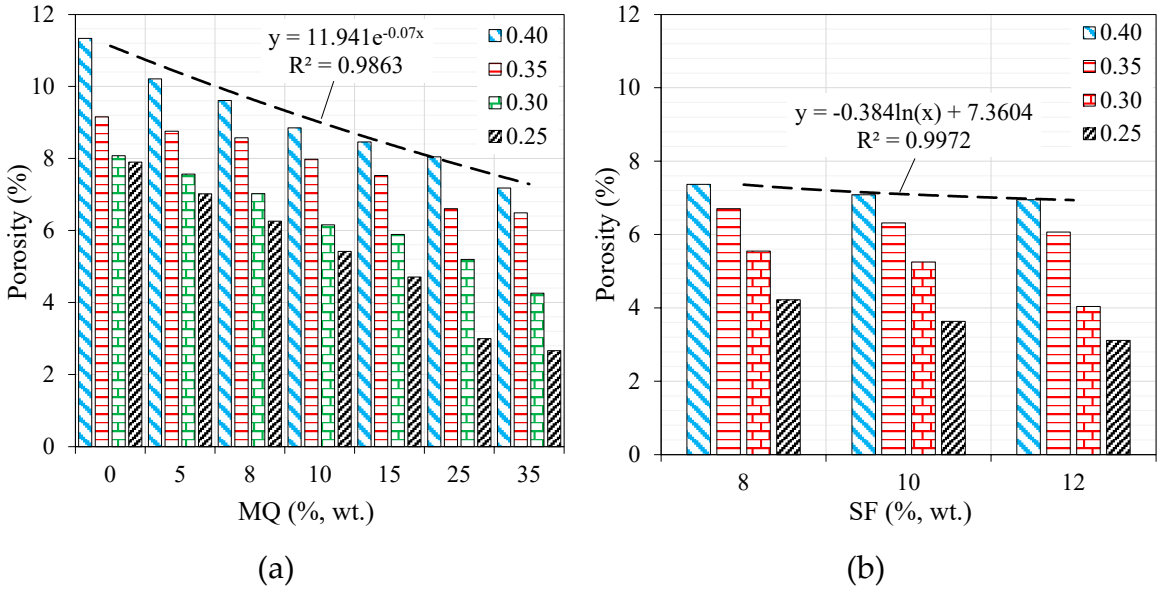

Figure 14. Porosity of: (a) MQ-, and (b) SF-concrete.

At varying water-binder ratios, the impact of the incorporation of SF into concrete on its porosity is illustrated in Figure 14b. As the water-binder ratio increased, the porosity increased throughout the matrix, with the maximum porosity observed at 0.4. A substantial reduction in matrix porosity has also been observed as a result of increased SF content. With higher water-binder ratios, the addition of SF to concrete mixtures resulted in a lesser increase in porosity, which can be attributed to the fewer micropores available since there was less cement in the mixture. The porosity improvement is more significant in mixtures with a lower water-to-cement ratio. The overall trend of a logarithmic function was observed in all mixtures with different levels of substitution of SF.

4.3. Effects of MQ and SF by statistical analysis

The analysis of variance (ANOVA) results at a confidence level of 95% for strength, porosity and RCPT are presented in Tables 6 and 7. The essential variables included the replacement level of ultrafine and w/b ratio, which significantly affect compressive strength, porosity, and accordingly permeability. As per the ANOVA results, the w/b ratio and the replacement level of ultrafine substantially both impact the values of compressive strength, porosity, and RCPT. The F-value found in the analysis of variance of experimental data was notably higher than F_{crit}, which means that water to cement ratio and parameters are significant for deciding the effective parameter as listed in Table 7.

Preprints (www.preprints.org) | NOT PEER-REVIEWED | Posted: 9 October 2023 doi:10.20944/preprints202310.0448.v1

Table 6. ANOVA analysis of the effect of different levels of MQ replacement.

Summary	Response	Sum	Average	Variance
w-b: 0.25	Strength	589.80	84.26	68.65
	Porosity	36.96	5.28	3.87
	Permeability	4814.67	687.81	270346.8
w-b: 0.30	Strength	512.31	73.18	54.68
	Porosity	44.17	6.31	1.80
	Permeability	6352	907.42	658373.8
w-b: 0.35	Strength	441.57	63.08	86.81
	Porosity	55.09	7.87	1.09
	Permeability	9121.16	1303.02	735011.5
w-b: 0.40	Strength	374.39	53.48	64.39
	Porosity	63.69	9.09	1.95
	Permeability	11431	1633	1113823

Table 7. ANOVA for MQ.

Source of Variation	SS	d_f	MS	F-value	P-value	F_{crit}
w/c ratio	26133897	11	2375809	13.79	3.05E-13	1.94
Properties	5297891	6	882981.9	5.12	0.0002	2.23
Error	11369141	66	172259.7			
Total	42800930	83				

Similarly, the ANOVA results at a confidence level of 95% for compressive strength, porosity, and RCPT are presented in Tables 8 and 9. The essential variables included SF and w/b ratio. The main goals of this part of the study are to investigate the effects of SF replacement level (8-12%) and w/b ratio on compressive strength, porosity, and RCPT values. The F-value found in the analysis of variance of experimental data was significantly more than F_{crit} (Table 9) which means that water to cement ratio and parameters are significant for deciding the effective parameter.

Table 8. ANOVA analysis of the effect of different levels of SF replacement.

Summary	Variable	Sum	Average	Variance
w-b: 0.25	Strength	284.75	94.91	10.00
	Porosity	10.96	3.65	0.30
	Permeability	718	239.33	8353.77
w-b: 0.30	Strength	247.64	82.54	12.46
	Porosity	14.83	4.94	0.63
	Permeability	1059	353	2860.33
w-b: 0.35	Strength	225.54	75.18	5.13
	Porosity	19.08	6.36	0.10
	Permeability	1429.66	476.55	2497.92
w-b: 0.10	Strength	199.72	66.57	8.61
	Porosity	21.39	7.13	0.046
	Permeability	2374	791.33	3155.11

Preprints (www.preprints.org) | NOT PEER-REVIEWED | Posted: 9 October 2023 doi:10.20944/preprints202310.0448.v1

Table 9. ANOVA for SF.

Source of Variation	SS	d_f	MS	F-value	P-value	$F_{crit.}$
Rows	1972030	11	179275.4	162.27	2.06E-18	2.26
Columns	9504.37	2	4752.18	4.30	0.026	3.44
Error	24304.56	22	1104.75			
Total	2005839	35				

4.4. Optimization of concrete mixtures

A representation of the strength and permeability responses for the various developed MQ concrete mixtures is shown in Figure 15. Based on the figure, a replacement level of 8% MQ led to a reduction in compressive strength. In general, the results indicate that concrete containing 8% MQ and 0.3 water-binder ratio had improved compressive strength and durability properties.

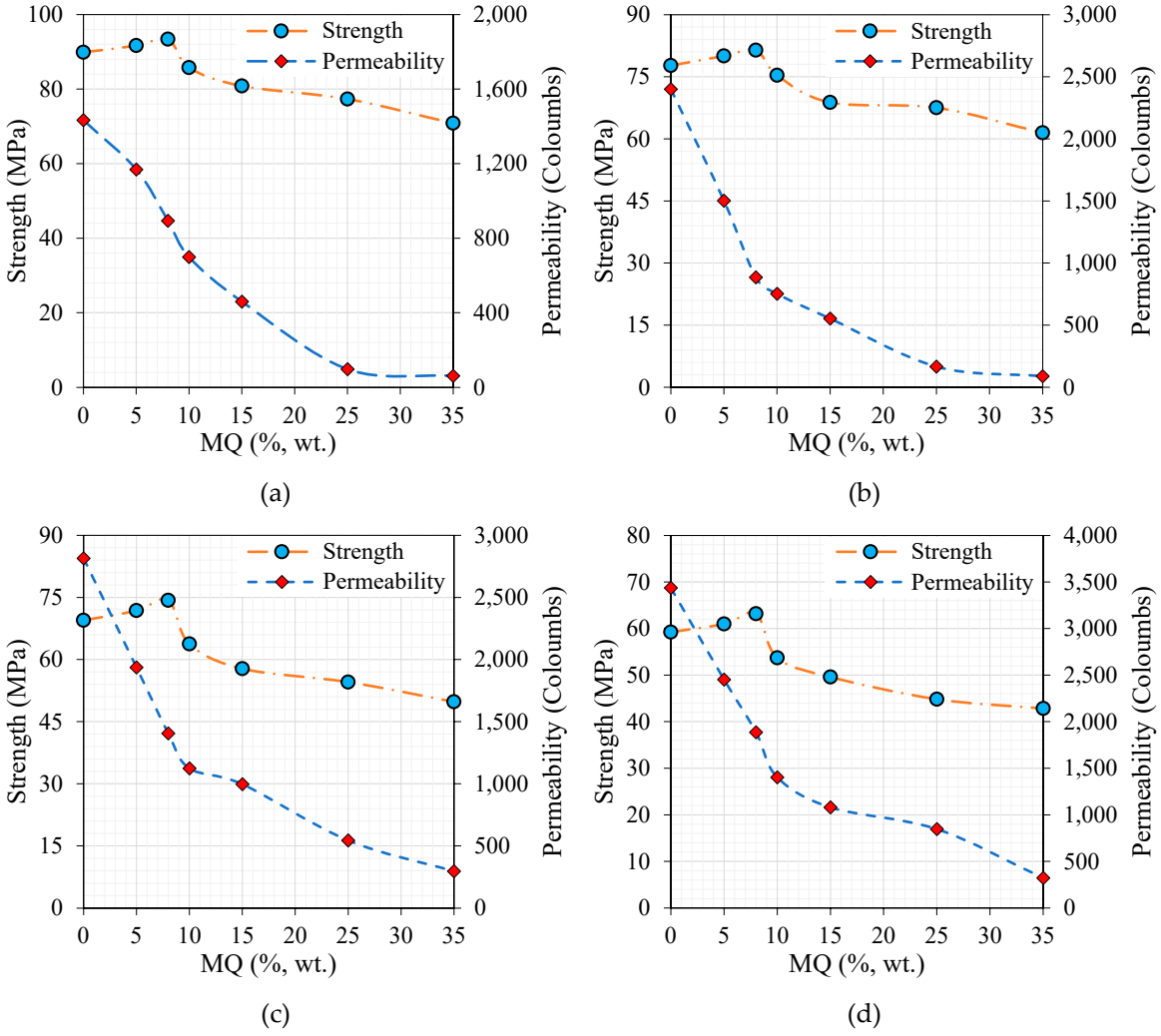

Figure 15. Strength and permeability responses for the various developed MQ concrete mixtures with a w/b ratio of: (a) 0.25, (a) 0.30, (a) 0.35, and (b) 0.40.

Preprints (www.preprints.org) | NOT PEER-REVIEWED | Posted: 9 October 2023 doi:10.20944/preprints202310.0448.v1

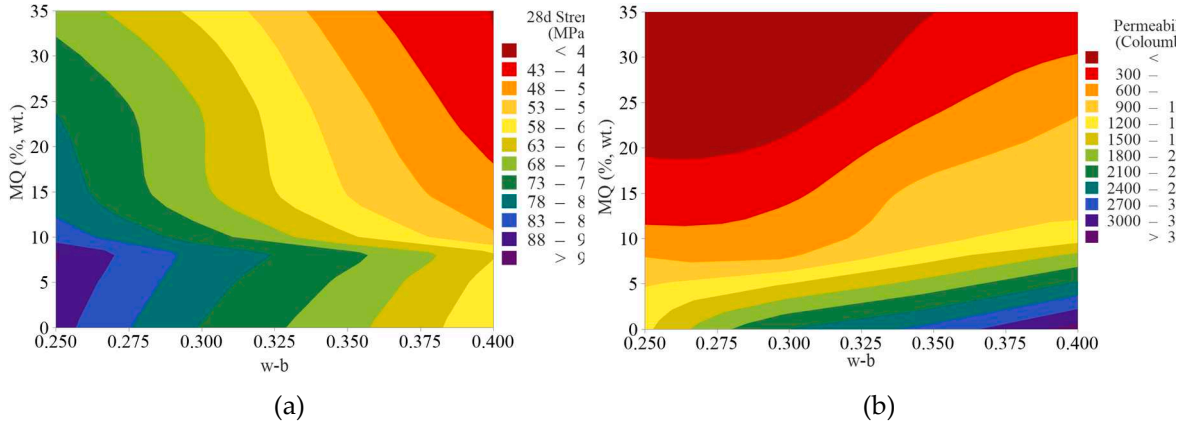

(a) (b)

Figure 16. (a) strength and (b) permeability contour plots for the MQ concrete mixtures.

5. Conclusions, limitations, and future directions

The use of ultrafine fillers and superplasticizers in the packing of materials can improve the freshness, mechanical properties, and durability of concrete. There is however a need for further research on ultrafine fillers as well as an admixture of pozzolanic minerals in a ternary blend of fillers. Moreover, there is an urgent need to carry out evaluating research to investigate the effects of ultrafine fillers derived from inert material on the durability of high-strength concrete. From the results, it is concluded that MQ can contribute to compressive strength, porosity, and permeability in a similar way to SF. This improvement was attributed to its ultrafine particles that support the filling effect and the packing density of the cementitious matrix.

(1) Regardless of the type of fine material, porosity, and permeability, both decrease as the replacement level rises.
(2) The strength improves with the SF level, while it shows a maximal value at MQ of 25%.
(3) All SF mixes had the highest strength, and in the case of MQ, it remained the highest until a replacement level of 15%.
(4) In a manner similar to SF, the ultrafine size of MQ particles improves compressive strength, porosity, and permeability despite having a high degree of crystallinity.

Building upon this research, the following are some potential prospects and directions. To strike a harmonious equilibrium between mechanical attributes and cost-effectiveness, there is room for refining the replacement proportions of SF and MQ. Furthermore, a comprehensive evaluation of the system's life cycle and sustainability implications is imperative. Lastly, exploring the viability of integrating nanomaterials like nano-silica or nano-alumina into binary cementitious systems warrants thorough investigation.

Acknowledgments: The authors extend their appreciation to Researcher Supporting Project number (RSPD2023R692), King Saud University, Riyadh, Kingdom of Saudi Arabia.

References

1. Initiative Cement Sustainability (CSI). Recycling Concrete. World Business Council for Sustainable Development-WBCSD. 2009.
2. Aıtcin P. The durability characteristics of high performance concrete: a review. Cement and concrete composites. 2003;25(4-5):409-420.
3. Stroeven M. Discrete numerical modelling of Composite Materials-application to cementitious materials. Delft, The Netherlands: Delft University of Technology; 1999.
4. Bai G, Wang L, Ma G, et al. 3D printing eco-friendly concrete containing under-utilised and waste solids as aggregates. Cement and Concrete Composites. 2021;120:104037.
5. Zhou Y, Guo D, Xing F, et al. Multiscale mechanical characteristics of ultra-high performance concrete incorporating different particle size ranges of recycled fine aggregate. Construction and Building Materials. 2021;307:125131.

6. Bui D, Hu J, Stroeven P. Particle size effect on the strength of rice husk ash blended gap-graded Portland cement concrete. Cement and concrete composites. 2005;27(3):357-366.
7. Zhang H, Ji T, Liu H. Performance evolution of the interfacial transition zone (ITZ) in recycled aggregate concrete under external sulfate attacks and dry-wet cycling. Construction and Building Materials. 2019;229:116938.
8. Zhao H, Wu Z, Liu A, et al. Numerical insights into the effect of ITZ and aggregate strength on concrete properties. Theor Appl Fract Mech. 2022;120:103415.
9. Lagerblad B, Kjellsen K. Normal and high strength concretes with conventional aggregates. RILEM REPORT. 1999:53-70.
10. Kaufmann J, Winnefeld F, editors. Influence of addition of ultrafine cement on the rheological properties and strength of Portland cement paste. Innovations and Developments In Concrete Materials And Construction: Proceedings of the International Conference held at the University of Dundee, Scotland, UK on 9–11 September 2002; 2002: Thomas Telford Publishing.
11. Bayramov F, Tasdemir M, Ilki A, et al., editors. Steel fibre reinforced concrete for heavy traffic load conditions. Proceedings of the 9th International Symposium on Concrete Roads, Istambul, Turkey; 2004.
12. Neville AM. Properties of concrete. Vol. 4. England: Pearson; 2004.
13. Dobiszewska M, Schindler AK, Pichór W. Mechanical properties and interfacial transition zone microstructure of concrete with waste basalt powder addition. Construction and Building Materials. 2018;177:222-229.
14. Adamu M, Ibrahim YE, Al-Atroush ME, et al. Mechanical properties and durability performance of concrete containing calcium carbide residue and nano silica. Materials. 2021;14(22):6960.
15. Mazloom M, Ramezanianpour A, Brooks J. Effect of silica fume on mechanical properties of high-strength concrete. Cement and concrete composites. 2004;26(4):347-357.
16. Güneyisi E, Gesoğlu M, Karaoğlu S, et al. Strength, permeability and shrinkage cracking of silica fume and metakaolin concretes. Construction and Building Materials. 2012;34:120-130.
17. Shi H-s, Xu B-w, Zhou X-c. Influence of mineral admixtures on compressive strength, gas permeability and carbonation of high performance concrete. Construction and Building Materials. 2009;23(5):1980-1985.
18. Behnood A, Ziari H. Effects of silica fume addition and water to cement ratio on the properties of high-strength concrete after exposure to high temperatures. Cement and Concrete Composites. 2008;30(2):106-112.
19. Wong H, Razak HA. Efficiency of calcined kaolin and silica fume as cement replacement material for strength performance. Cement and Concrete research. 2005;35(4):696-702.
20. Barger GS, Hill RL, Ramme BW, et al. Use of fly ash in concrete. American Concrete Institute, Farmington Hills, MI, USA. 2003.
21. Papadakis VG. Effect of fly ash on Portland cement systems: Part I. Low-calcium fly ash. Cement and concrete research. 1999;29(11):1727-1736.
22. Poon CS, Kou S, Lam L, et al. Activation of fly ash/cement systems using calcium sulfate anhydrite (CaSO4). Cement and Concrete research. 2001;31(6):873-881.
23. Russell M, Basheer P, Rao J. Potential use of spent mushroom compost ash as an activator for pulverised fuel ash. Construction and Building Materials. 2005;19(9):698-702.
24. Zhang J, Lv T, Hou D, et al. Synergistic effects of fly ash and MgO expansive additive on cement paste: Microstructure and performance. Construction and Building Materials. 2023;371:130740.
25. Hanif A, Lu Z, Li Z. Utilization of fly ash cenosphere as lightweight filler in cement-based composites–A review. Construction and building materials. 2017;144:373-384.
26. Khan M. Permeation of high performance concrete. J Mater Civ Eng. 2003;15(1):84-92.
27. Yazıcı H. The effect of curing conditions on compressive strength of ultra high strength concrete with high volume mineral admixtures. Building and environment. 2007;42(5):2083-2089.
28. Demirboğa R. Thermal conductivity and compressive strength of concrete incorporation with mineral admixtures. Building and Environment. 2007;42(7):2467-2471.
29. Nochaiya T, Wongkeo W, Chaipanich A. Utilization of fly ash with silica fume and properties of Portland cement–fly ash–silica fume concrete. Fuel. 2010;89(3):768-774.
30. Azmee N, Abbas YM, Shafiq N, et al. Enhancing the microstructure and sustainability of ultra-high-performance concrete using ultrafine calcium carbonate and high-volume fly ash under different curing regimes. Sustainability. 2021;13(7):3900.
31. Abbas YM, Khan MI. Optimization of Arabian-Shield-Based Natural Pozzolan and Silica Fume for High-Performance Concrete Using Statistical Design of Experiments. Adv Civ Eng. 2021 2021/04/08;2021:5512666.
32. Abbas Y. Simplex-lattice strength and permeability optimization of concrete incorporating silica fume and natural pozzolan. Construction and Building Materials. 2018;168:199-208.
33. Khan MI, Abbas YM. Curing optimization for strength and durability of silica fume and fuel ash concretes under hot weather conditions. Construction and Building Materials. 2017;157:1092-1105.

34. Khan MI, Abbas YM. Robust Extreme Gradient Boosting Regression Model for Compressive Strength Prediction of Blast Furnace Slag and Fly Ash Concrete. Materials Today Communications. 2023:105793.
35. Bouzoubaa N, Bilodeau A, Sivasundaram V, et al. Development of ternary blends for high-performance concrete. Materials Journal. 2004;101(1):19-29.
36. Özyıldırım C, Halstead W. Improved concrete quality with combinations of fly ash and silica fume. ACI Materials Journal. 1994;91(6):587-594.
37. Ronne M. Effect of condensed silica fume and fly ash on compressive strength development of concrete. Special Publication. 1989;114:175-190.
38. Abed M, Nemes R. Long-term durability of self-compacting high-performance concrete produced with waste materials. Construction and Building Materials. 2019;212:350-361.
39. Bakker R. Application and advantages of blended cement concretes. QCL Group Technical Note. 1999.
40. Moosberg-Bustnes H, Lagerblad B, Forssberg E. The function of fillers in concrete. Materials and Structures. 2004;37:74-81.
41. Nehdi M. Microfiller effect on rheology, microstructure, and mechanical properties of high-performance concrete. The University of British Columbia: National Library of Canada= Bibliothèque nationale du Canada, Ottawa; 1999.
42. Fennis S. Design of ecological concrete by particle packing optimization. the Netherlands: University of Technology; 2011.
43. Vogt C. Ultrafine particles in concrete: Influence of ultrafine particles on concrete properties and application to concrete mix design: Royal Institute of Technology; 2010.
44. Cyr M, Lawrence P, Ringot E. Mineral admixtures in mortars: Quantification of the physical effects of inert materials on short-term hydration. Cement and concrete research. 2005;35(4):719-730.
45. Shi C, Wu Z, Xiao J, et al. A review on ultra high performance concrete: Part I. Raw materials and mixture design. Construction and Building Materials. 2015;101:741-751.
46. Mehdipour I, Khayat KH. Effect of particle-size distribution and specific surface area of different binder systems on packing density and flow characteristics of cement paste. Cement and Concrete Composites. 2017;78:120-131.
47. Yousuf S, Sanchez L, Shammeh S. The use of particle packing models (PPMs) to design structural low cement concrete as an alternative for construction industry. Journal of Building Engineering. 2019;25:100815.
48. Kosmatka SH, Kerkhoff B, Panarese W. Fly ash, slag, silica fume, and natural pozzolans. Design and control of concrete mixtures. 2002;13:57-72.
49. Zagar L, editor Methods of determination of pore structure, permeability and diffusion. Proceedings of RILEM / IUPAC International Symposium on the Pore Structure and Properties of Materials; 1973; Prague.
50. Cheerarot R, Tangpagasit J, Jaturapitakkul C. Compressive strength of mortars due to pozzolanic reaction of fly ash. Special Publication. 2004;221:411-426.
51. Jaturapitakkul C, Tangpagasit J, Songmue S, et al. Filler effect and pozzolanic reaction of ground palm oil fuel ash. Construction and Building Materials. 2011;25(11):4287-4293.
52. Khan M, Abbas Y, Fares G. Review of high and ultrahigh performance cementitious composites incorporating various combinations of fibers and ultrafines. Journal of King Saud University-Engineering Sciences. 2017;29(4):339-347.
53. Wang X, Wu D, Zhang J, et al. Design of sustainable ultra-high performance concrete: A review. Construction and Building Materials. 2021;307:124643.
54. Kirthika S, Singh S, Chourasia A. Alternative fine aggregates in production of sustainable concrete-A review. Journal of cleaner production. 2020;268:122089.
55. Loland K, Hustad T. Report 2 Mechanical Properties. FCB/SINTEF. 1981.
56. Sellevold EJ, Nilsen T. Condensed silica fume in concrete: a world review. Supplementary Cementing Materials for concrete CANMET; Ottawa, Canada1987. p. 165-243.
57. Newman J, Choo BS. Advanced concrete technology 2: concrete properties. Elsevier; 2003.
58. Benli A, Karataş M, Bakir Y. An experimental study of different curing regimes on the mechanical properties and sorptivity of self-compacting mortars with fly ash and silica fume. Construction and Building Materials. 2017;144:552-562.
59. Lamond JF, Pielert JH. Significance of tests and properties of concrete and concrete-making materials. Vol. 169. ASTM international; 2006.
60. Scrivener KL, Juilland P, Monteiro PJ. Advances in understanding hydration of Portland cement. Cement and Concrete Research. 2015;78:38-56.
61. Abrams L. Properties of concrete. Pitman Publishing Ltd.: London, UK; 1919.
62. Oluokun FA. Fly ash concrete mix design and the water-cement ratio law. Materials Journal. 1994;91(4):362-371.
63. Abd Elaty MAA. Compressive strength prediction of Portland cement concrete with age using a new model. HBRC journal. 2014;10(2):145-155.

64. Taerwe L. Constitutive modelling of high strength/high performance concrete: state-of-art report. Vol. 42. Fédération internationale du Béton (FIB); 2008.
65. Mehta PK, Monteiro PJ. Concrete: microstructure, properties, and materials. McGraw-Hill Education; 2014.
66. Burg R, Ost B. Engineering properties of commercially available high-strength concretes (including three-year data). 1994.
67. Hu J, Ge Z, Wang K. Influence of cement fineness and water-to-cement ratio on mortar early-age heat of hydration and set times. Construction and building materials. 2014;50:657-663.
68. Qi T, Zhou W, Liu X, et al. Predictive hydration model of Portland cement and its main minerals based on dissolution theory and water diffusion theory. Materials. 2021;14(3):595.
69. Shen D, Wang X, Wu S. Determining hydration mechanisms for initial fall and main hydration peak in tricalcium silicate hydration using a two-scale hydration simulation model. Cement and Concrete Research. 2022;156:106763.
70. Detwiler RJ, Mehta PK. Chemical and physical effects of silica fume on the mechanical behavior of concrete. Materials Journal. 1989;86(6):609-614.
71. Goldman A, Bentur A. Properties of cementitious systems containing silica fume or nonreactive microfillers. Advanced Cement Based Materials. 1994;1(5):209-215.
72. Ibrahim RK, Hamid R, Taha M. Strength and Microstructure of Mortar Containing Nanosilica at High Temperature. ACI Materials Journal. 2014;111(2).
73. Amin M, Zeyad AM, Tayeh BA, et al. Effect of ferrosilicon and silica fume on mechanical, durability, and microstructure characteristics of ultra high-performance concrete. Construction and Building Materials. 2022;320:126233.